Experimental Validation of SPAMM Tagged Magnetic Resonance Imaging Based Measurement of Non-uniform 3D Soft Tissue Deformation

K. M. Moerman[1,2], C. K. Simms[1], A. M. Sprengers[2], J. Stoker[2], and A. J. Nederveen[2]
[1]Trinity Centre for Bioengineering, Trinity College Dublin, Dublin, Ireland, [2]Radiology, Academic Medical Centre, Amsterdam, Netherlands

Introduction

Assessment of the deformation of human soft tissue is vital in diverse applications such as biomechanics and the study of bowel motility. However, deriving deformation from MRI is complex and the methods employed require validation. For this study a novel Magnetic Resonance Imaging (MRI) sequence, based on SPAtial Modulation of the Magnetization (SPAMM) designed for real-time measurement of non-periodic movements was evaluated for its ability to measure 3D soft tissue deformation. The deformation derived from SPAMM tagged MRI was validated using marker tracking in a silicone gel phantom.

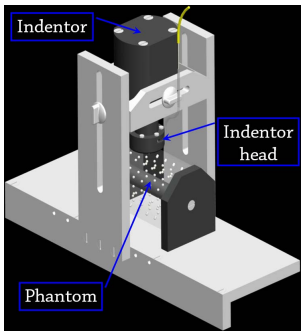

Figure 1. The ELD and soft tissue phantom

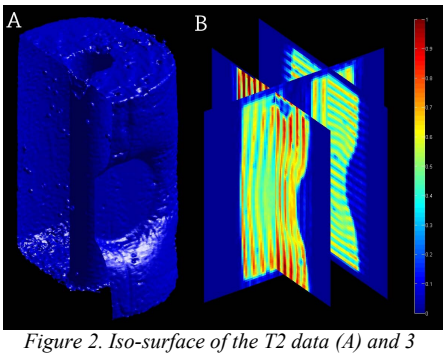

Figure 2. Iso-surface of the T2 data (A) and 3 image slices for the orthogonal tag data (B)

Materials and methods

The validation set-up: indentor and soft tissue phantom. A MRI compatible indentor (figure 1) was used to apply static indentation to a silicone gel soft tissue phantom containing contrasting spherical polyoxymethylene markers 3±0.05 mm in diameter. The phantom is cylindrical (200 mm long and 120 mm in diameter) with a stiff bone-like core and was indented transversely (~20 mm deep) using a circular indentor. Figure 2a is an iso-surface of a section of the deformed phantom showing the circular indentation site and some of the markers inside. Tracking of these markers provides an independent measure of deformation allowing for the validation of the SPAMM tagged MRI (figure 2b) based deformation measurement [1]. The silicone gel has similar MRI [2] and mechanical [3] properties to human soft tissue.

MRI sequence design. The SPAMM pre-pulse imposes a line pattern on the magnetization, the distortion of which can be directly related to the motion that occurred between pre-pulse and readout. For the current study a SPAMM sequence was reconfigured for measurement of phantom indentation by removing the external trigger dependence and acquiring a full readout after the indention. The scans were performed on a 3.0 Tesla Philips Intera scanner using two FLEX-M coils and a Turbo Field Echo (TFE) readout, scan parameters: T_R/T_E=2.9/1.8 ms, flip angle 8°, field of view (FOV) 130x130x67.5 mm, 45 slices, voxel size 1.35x1.35x1.5 mm. The SPAMM tagged MRI data was acquired in 3 orthogonal directions (see figure 2b). The marker locations were determined from high resolution (0.5 mm isotropic) T2-weighted scans of the same FOV.

Deriving and comparing deformation from the MRI data. To derive deformation from the SPAMM tagged MRI data, tags were represented as cubic spline surfaces. These tag surfaces (figures 3a-c) were segmented using masking and a sheet marching algorithm. Figure 3d illustrates the tag surfaces from all 3 directions. The intersections of these surfaces provide a 3D grid of trackable points. Using interpolation the marker locations in the deformed configurations can be predicted. Calculation of the difference between the predicted and measured marker locations allows for the validation of the SPAMM tagged MRI derived deformation measures. The marker locations in the T2-weighted scans were determined using the methods outlined in [1].

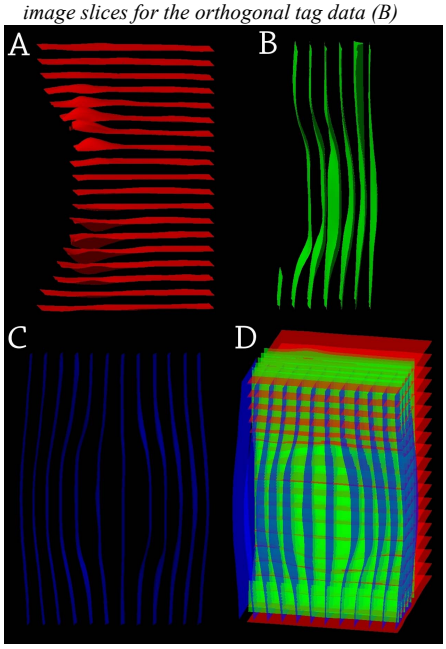

Figure 3. MRI data with segmented surfaces in transverse (A), coronal (B) and sagittal direction (C). The combined surfaces (D).

Results and Discussion

Following calculation of the intersections of the tag surfaces, segmented from the SPAMM tagged MRI data, the displacement vector field shown in figure 4a was obtained. Using this field and knowledge of the original marker locations (blue points in figure 4a and b) the marker locations in the deformed configuration were predicted (red points in figure 4b). Figure 4b demonstrates that the true (green points) and predicted marker locations in the deformed configuration largely overlap. The errors in the x, y and z directions are approximately normally distributed and the total error magnitude range is 0.19~2.6 mm (mean: 0.75 mm, standard deviation: 0.61 mm). This error is mainly due to the excessive deformation applied and the phantom geometry used. The largest errors occurred either at the edge of the displacement field (e.g. the point circled in red in figure 4b) where predictions are made with only limited information, or in locations where the appearance of tags was poor due to excessive compression against the bone-like core in the phantom and due to orthogonal stretching of the tags resulting in loss of tag contrast. Since in these locations the surface segmentation was more challenging (or unsuccessful, e.g. first surface in figure3b) less or less accurate deformation information was available for the prediction of the marker locations. Excluding these (3) points from the error analysis leads to an error magnitude range of 0.19~0.95 mm (mean: 0.53 mm, standard deviation: 0.25 mm). The errors can be further reduced by applying less extreme deformation, allowing more surfaces to be segmented with higher accuracy, resulting in a better prediction of marker locations.

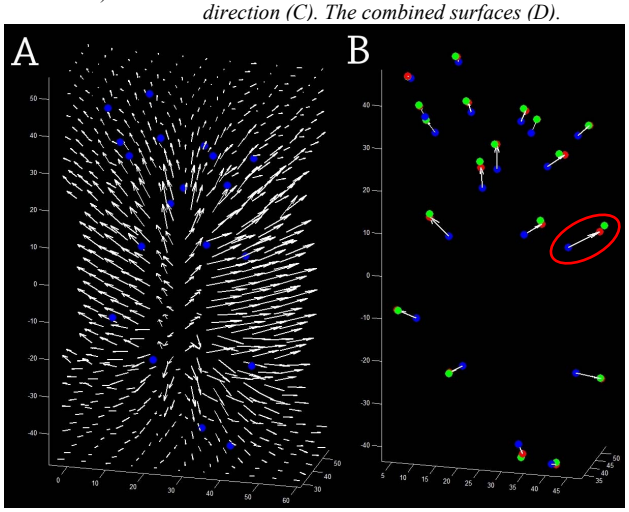

Figure 4. The 3D displacement vector field and original marker locations (blue) (A) and the un-deformed (blue), deformed (green) and predicted marker locations (red) (B)

Conclusion

The use of a novel non-triggered tagged MRI sequence, based on SPAMM and designed for real-time measurement of non-periodic movements, to record static deformations was evaluated using marker tracking in a silicone gel phantom. With the current phantom the mean error is 0.75 mm. However this can be reduced to under 0.53 mm if the indentation depth is reduced allowing for the optimisation of the tag surface segmentation and marker location prediction.

References

[1] Moerman, K.M. et al, EURASIP Journal on Advances in Signal Processing. 2010. **[2]** Goldstein, D.C. et al, Invest. Radiol, 1987. 22(2): p.153-7. **[3]** Moerman, K.M et al. Journal of Biomechanics. 2009 42(8): p.1150-1153.